THE GEOLOGICAL SOCIETY OF AMERICA®

Climatically driven formation of the Tangxian planation surface in North China: An example from northwestern Zhongtiao Shan of the Shanxi Graben System

Jianguo Xiong[1,2,*], Youli Li[2], Wenjun Zheng[1], Peizhen Zhang[1], Jinghao Lei[2], Yuezhi Zhong[2,3], Xiu Hu[2], Zhigang Li[1], Zheng Gong[1], Tao Li[1], Yipeng Zhang[1], Binbin Xu[1], Qingying Tian[1], Weilin Xin[2], Xiaolin Ren[2], and Yifan Yao[4]

[1]GUANGDONG PROVINCIAL KEY LABORATORY OF GEODYNAMICS AND GEOHAZARDS, SCHOOL OF EARTH SCIENCES AND ENGINEERING, SUN YAT-SEN UNIVERSITY, GUANGZHOU, 510275, CHINA
[2]KEY LABORATORY OF EARTH SURFACE PROCESSES OF MINISTRY OF EDUCATION, PEKING UNIVERSITY, BEIJING 100871, CHINA
[3]DEPARTMENT OF EARTH SCIENCES, ETH ZURICH, SONNEGGSTRASSE 5, 8092 ZURICH, SWITZERLAND
[4]COLLEGE OF URBAN AND ENVIRONMENTAL SCIENCES, PEKING UNIVERSITY, BEIJING 100871, CHINA

ABSTRACT

The development of planation surfaces requires stable tectonic and climatic conditions. However, it is difficult to discuss in detail how tectonic movement and/or climate change affects erosion, deposition, and uplift associated with the development, formation, and disintegration of planation surface. This article presents a case study on the development and formation of the Tangxian planation surface (TXPS) by establishing the magnetostratigraphy of one piedmont deposition section related to planation, and combining the depositional sequence overlying TXPS and basin sediments. Further, we discuss the role of tectonics and climate change in the geomorphic evolution of the TXPS during the late Cenozoic and revise the final formation age to be ca. 3.1 Ma by the relative deposition process. The vertical rates of the main fault constrained by different geomorphic surfaces and stable deposition in the basin show stable and moderate tectonic activity in the study area since the Pliocene, and a series of sedimentary records reveal that the climate in North China was stably warm-humid from the late Miocene to early Pliocene. Stable tectonic activity and stable climate were important bases for pediment development; however, abrupt climatic changes during the late Pliocene might be the main driving force of the final formation of the TXPS in North China.

LITHOSPHERE; v. 10; no. 4; p. 530–544 | Published online 16 May 2018 https://doi.org/10.1130/L720.1

INTRODUCTION

In geomorphology, extensive topographical surfaces that cut across bedrock structures with low relief and low slope gradients are known as *planation surfaces* (Goudie, 2004). This includes peneplains, pediments, pediplains, and etchplains (Adams, 1975; Cui et al., 1999). Such surfaces crosscut all the older strata as intersecting surfaces (Coltorti and Pieruccini, 2000; Wu, 2008). Three main constraints on the development, formation, and persistence of planation surfaces include (i) the length of quiescence between two crustal tectonic uplift periods; (ii) sea level fluctuations; and (iii) the intensity of post-quiescent rising and degree of cutting (Tator, 1952; Wu, 2008; Phillips, 2002). How do tectonics and/or climate change play roles in the development, formation, uplift, and disintegration of planation surface? It is difficult to address this question because the direct relationship between erosion and staged tectonic uplift or climate change is not easily established (Reynaud et al., 1999; Casas-Sainz and Cortés-Gracia, 2002).

*Corresponding author: xiongjg@pku.edu.cn

The interplay of tectonics, climate, deposition, and erosion results in a complex evolution of paleolandscapes and planation surfaces (Phillips, 2002, 2006; Rossetti, 2004). Tectogenesis controlled the planation surface to be uplifted several hundred meters or even several kilometers above sea level. However, no direct evidence reveals this process. Tectonic instability theory and sea level perturbations are explanations for the paucity of peneplains (Phillips, 2002). On the contrary, the intermittent tectonic activity or climate fluctuation can interpret the existence of the multiple pediment levels (Tator, 1952). Numerical process-response modeling indicates that lithologically and structurally variable basement regions are not likely to favor the development of planation surfaces (Römer, 2010), and a planation surface would be better preserved on harder rocks and in the higher parts of the local relief (Coltorti and Pieruccini, 2000). A planation surface with a multiphase history is unlikely to have chronostratigraphic significance (Evenstar et al., 2009). Based on these, the obstacles must be cleared for studying the development and formation of planation surfaces.

Here, we provide an example of planation surface study from the Zhongtiao Shan (ZTS; Shan means mountains in Chinese)–Yuncheng Basin, part of the southern Shanxi Graben System in North China (Fig. 1). One Tangxian planation surface (TXPS) is distributed in the northwestern ZTS. The relatively uniform lithology and structure are considered not to interfere with the planation process. The stability of the tectonic stress field (Li et al., 1998; Xie, 2004) and multilevel planation surfaces (Fig. 2; Wu, 2008) in the Cenozoic indicate that the TXPS does not have multi-period history. The Yuncheng Basin borehole reveals a complete deposition record since the Pliocene (Wang et al., 2002). From the base of sediments overlying the planation surface, the final formation age of the TXPS was constrained to 3.12–3.03 Ma (Fig. 3; Xiong et al., 2017). Here we present the magnetostratigraphy of the Wangyukou (WYK) section of the Xiaxian Conglomerate, a piedmont sedimentary sequence related to TXPS development. The final formation age of the TXPS will be revised by these sedimentary records. The vertical rates of the north ZTS fault, the boundary

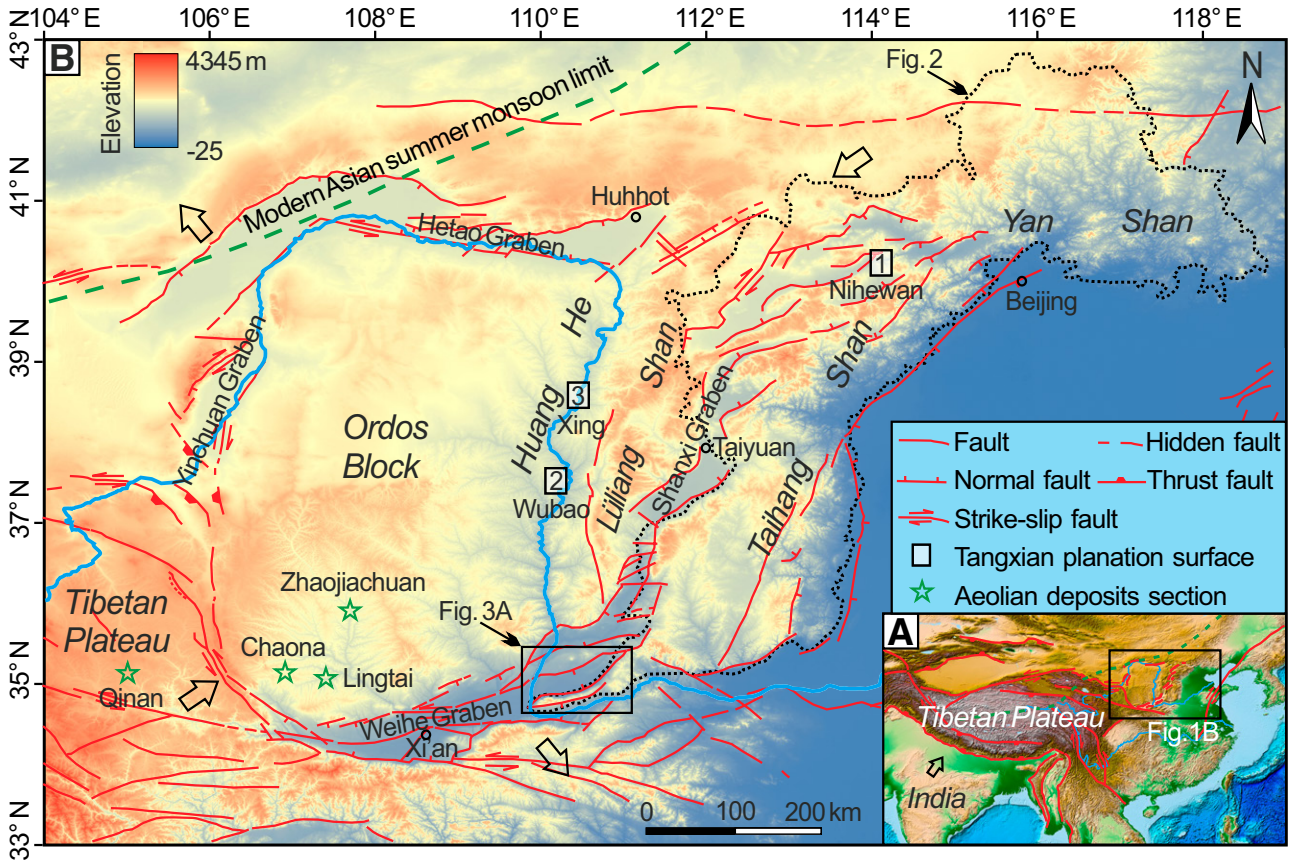

Figure 1. (A) Relationship between the regional epeirogenic uplift and the Tibetan Plateau uplift and Ordos region is in the stress field of NE to east to NNE principal horizontal compression during the late Cenozoic (Cheng et al., 2002; Deng et al., 2007). The upper and lower solid blue lines are the Huang He and Yangtze River, respectively. (B) Simplified tectonic map of the Ordos Block and Shanxi Graben System showing faults and four graben systems with faulted basins around the Ordos Block and locations of the referenced Tangxian planation surfaces and climate records from aeolian deposits sections. The distribution area of three planation surfaces is enclosed by a black-dotted line in North China. The pair of hollow arrows show principal compression or extension stress orientation. All the faults were active during the Quaternary. The green dashed line is the modern Asian summer monsoon limit (Chen et al., 2008).

fault between the ZTS and Yuncheng Basin, can be constrained by the TXPS, the Xiaxian Conglomerate surface, and the accumulation surfaces in the Yuncheng Basin corresponding to two geomorphic surfaces. In addition, a large number of reliable climate change curves in the late Cenozoic have been established on the aeolian deposits in North China, which is consistent with global climate change curves (An et al., 2001; Guo et al., 2002). Therefore, we can discuss in detail how tectonic movement and/or climate change affected erosion, deposition, and uplift associated with the development, formation, and disintegration of the TXPS.

GEOLOGIC SETTING

Tectonic and Geomorphic Setting

The North China Craton, located between the E-W–trending Yin Shan–Yan Shan Orogen in the north and the Qinling Orogen in the south, has experienced an ancient crystalline basement development of Archean to Paleoproterozoic age and a widespread Paleozoic and Mesozoic marine cover sedimentary stage (Zhai et al., 2011; Wang et al., 2014). In contrast, it experienced intense rifting events caused by crustal extension in the Cenozoic (Fig. 1B; Li et al., 1998; Lin et al., 2015). Since the Eocene, renewed tectonic activities have led to the formation of the Hetao Graben System, Yinchuan Graben System, Weihe Graben System, and subsidence of the North China Plain, now covered with exceedingly thick Cenozoic sediments (Li et al., 1998; Zhao et al., 2017). The Shanxi Graben System was formed from the Miocene to the early Pliocene, accompanied by the appearance of the Ordos Block (Li et al., 1998; Xie, 2004). The Ordos Block, located in the northeastern margin of the Tibetan Plateau, is influenced by the later northeast-directed extension (Fig. 1A; Zhang et al., 1991; Wang et al., 2014). The Ordos Block has been uplifted slowly and intermittently since the Eocene, with multiphase planation surfaces formed and preserved within it (Xu et al., 1993; Pan et al., 2012). The Lüliang Shan and Taihang Shan also experienced different uplift stages (Chen et al., 2012; Cao et al., 2015), and the multilevel planation surfaces are distributed over them (Wu, 2008).

Trilevel planation surfaces are distributed over the mountain areas in North China (Fig. 2; Wu, 2008). Beitai planation surfaces, the top surface of the high-altitude mountains, are distributed in the Wutai, Xiaowutai, and Lüliang Shans with an elevation of 2500–3050 m. Dianziliang planation surfaces are located in the top surfaces of the medium-altitude mountains with an elevation of 1500–2000 m. The TXPSs are divided into two types: pediment surfaces and hill surfaces. Pediment surfaces are distributed over piedmont areas with an elevation of 400–1400 m, and hill surfaces are distributed over mountain-front areas of the Taihang Shan and Yan Shan with an elevation of 50–600 m.

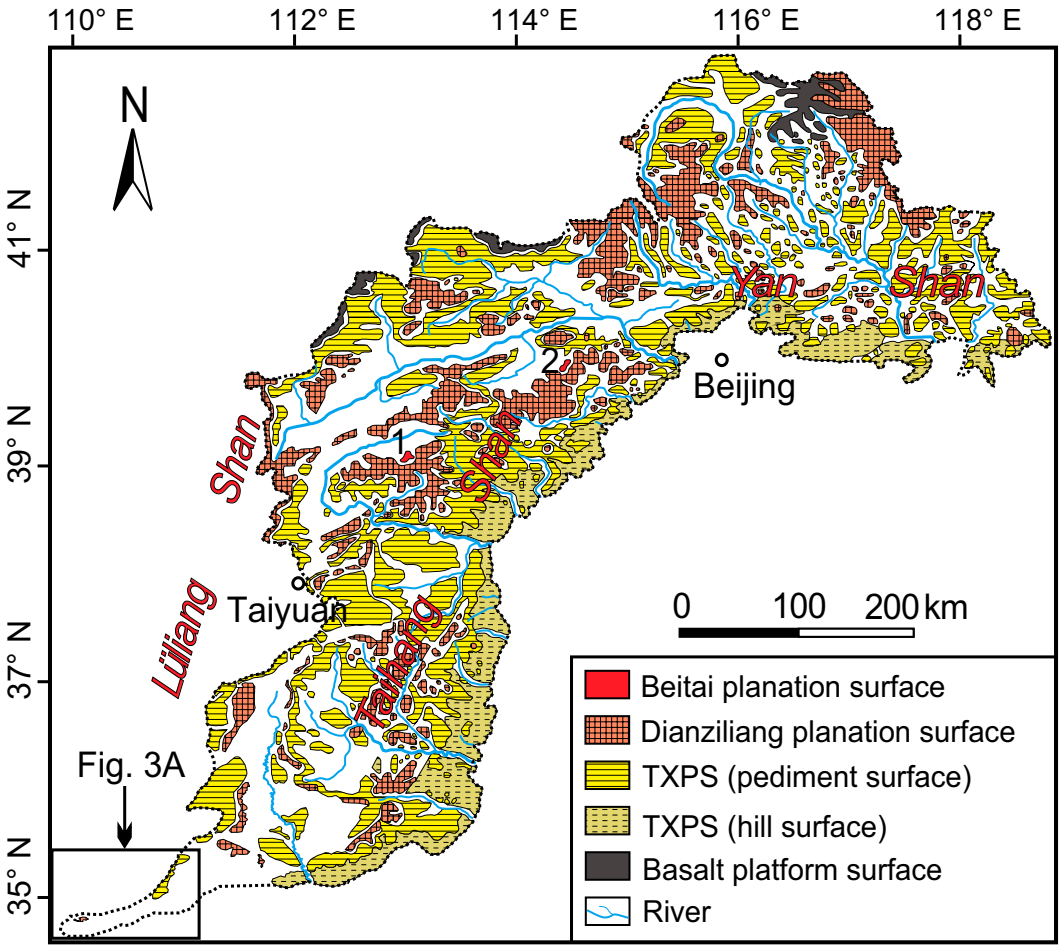

Figure 2. Distribution area of the Beitai, Dianziliang, and Tangxian planation surfaces of the mountain areas in North China modified from Wu (2008). 1—Wutai Shan; 2—Xiaowutai Shan; TXPS—Tangxian planation surface.

The Beitai surface and Dianziliang surface were formed in the late Cretaceous and the late Oligocene, respectively, constrained by ages of the latest rocks crosscut by these surfaces and the oldest overlying rocks (Willis et al., 1907; Wu, 2008). The summary of the TXPS studies in North China proposed the final formation ages of 3.6–2.6 Ma (Wu, 2008). More accurate data were given by recent magnetostratigraphy. The TXPS in the Nihewan area in the north Shanxi Graben System was formed at 3.1 Ma (Deng et al., 2008). The TXPSs in the Wubao and Xing areas in the Ordos Block were formed at 3.2 Ma (Liu et al., 2016) and 3.7 Ma (Pan et al., 2012), respectively.

The ZTS–Yuncheng Basin is located in the southernmost part of the Shanxi Graben System (Fig. 1B). The stratigraphic distributions include a metamorphic rock series of Paleoarchean and Proterozoic strata, Paleozoic marine sediments, and fluviolacustrine facies sediments and aeolian sediments in the Cenozoic (Fig. 3A; von Richthofen, 1882; Willis et al., 1907). In WYK Village, the northwestern ZTS has two geomorphic surfaces—the Xiaxian Platform and the Low Platform, with heights of 650–1000 m and ~500 m, respectively. The Xiaxian Platform consists of conglomerates and aeolian deposits of late Cenozoic age and the underlying TXPS and Xiaxian Conglomerate. The TXPS, actually the pediment surface, crosscut the Paleoarchean and Paleozoic strata (Figs. 3A and 3B). According to a study of its lithology, dominant direction of flat horizontal surfaces, roundness, and sorting features, the Xiaxian Conglomerate was considered to be piedmont deposits sourcing from the ZTS and might be related to the development and formation process of TXPS (Fig. 3; Wang et al., 1996). The WYK section is the best exposure of the Xiaxian Conglomerate. The contact relation between the Xiaxian Conglomerate and the pre-Cenozoic indicates the existence of fault F_1; in the northeast it converges with the main north ZTS fault. No displacement in the Xiaxian Conglomerate and overlying loess has been found, and the Xiaxian Conglomerate surface and the TXPS have the similar heights. The phenomena indicate that before the Xiaxian Conglomerate deposited or in the same period, the activities of fault F_1 led to uplift of the pre-Cenozoic rocks and made the WYK area a piedmont to receive sediments, and it has been inactive since the conglomerate deposition was ended. Faults F_2 and F_3 are the boundaries of the Xiaxian Platform, Low Platform, and Yuncheng Basin. All three faults are branches of the north ZTS fault (Fig. 3). There are three more faults in the basin—the E'meiling fault, the Mingtiaogang fault, and the Yanhu fault (Fig. 3A; Li et al., 1998; Wang et al., 2002). The north ZTS fault separates the ZTS and the Yuncheng Basin (Lv et al., 2014; Xiong et al., 2016a, 2017) and makes the Salt Lake area a depocenter with Cenozoic deposits more than 5 km thick (Xu et al., 1993).

Climate Setting Since the Late Miocene

North China is located in the Asian monsoon area (Fig. 1). A series of sedimentary records reveal that the climate in East Asia was stably warm-humid from the late Miocene to early Pliocene, consistent with global climate. The steady change of the benthic oxygen isotope record in South China Sea (Tian et al., 2008) is very similar to that in global oceans (Zachos et al., 2001). The summer monsoon index (Sun et al., 2010) and the magnetic susceptibility of the

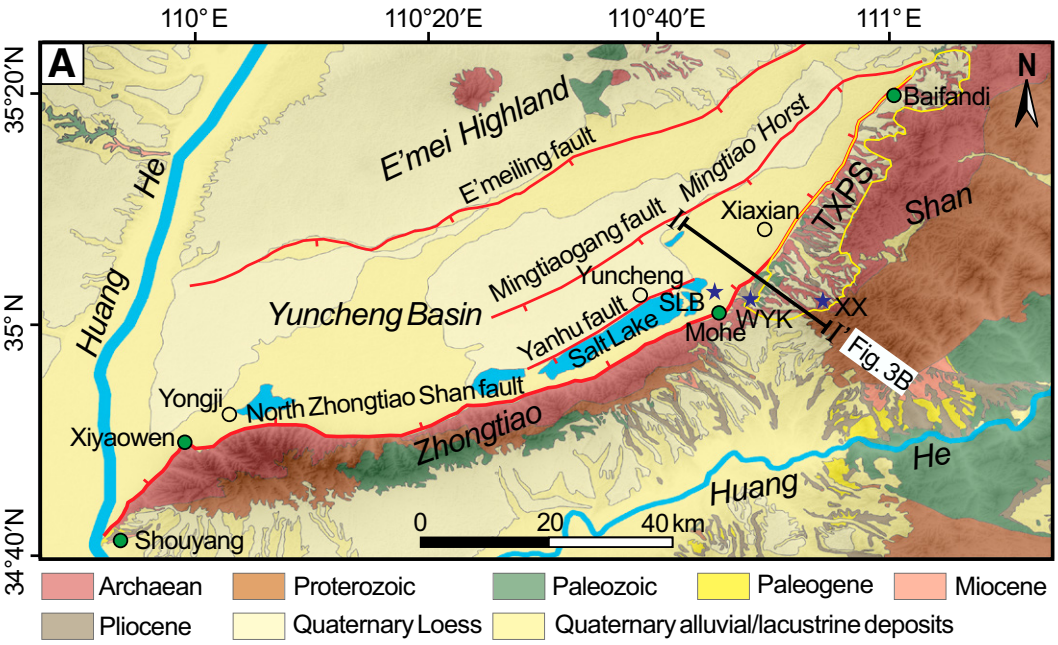

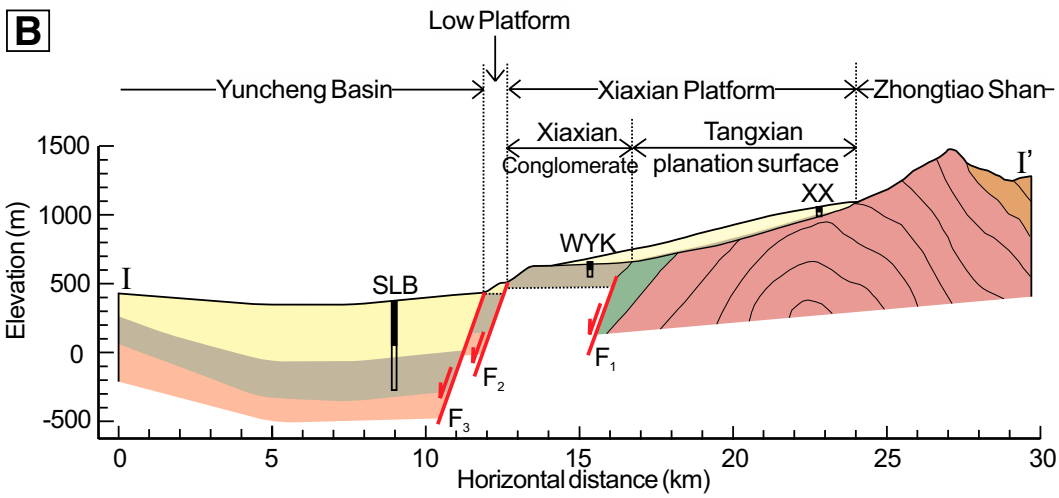

Figure 3. (A) Simplified geological map of the Yuncheng Basin and Zhongtiao Shan (ZTS, Shan means mountains in Chinese) digitized from 1:200,000 Chinese geologic maps (Ministry of Geology and Mineral Resources), with geomorphic units and main faults (Li et al., 1998; Wang et al., 2002). The yellow frame and five-pointed stars are positions of the Tangxian planation surface (TXPS) and magnetostratigraphic sections, respectively. WYK—Wangyukou; XX—Xiaxian (Xiong et al., 2017); SLB—Salt Lake borehole (Wang et al., 2002). (B) Geological cross section of the ZTS–Yuncheng Basin digitized from geologic maps. The Xiaxian Platform is composed of the Tangxian planation surface, Xiaxian Conglomerate, and overlying loess. The thickness of Pliocene and Quaternary strata in the Yuncheng Basin is constrained by the SLB and Mingtiaogang borehole sections (Wang et al., 2002). The thickness of Pliocene strata of the Low Platform is consistent with that of the Salt Lake borehole. The thickness of other strata in late Cenozoic is measured by this work, the thickness of Miocene strata is unknown, and the dotted line indicates the unknown boundary. (C) View of the TXPS, Xiaxian Platform, Low Platform, and Yuncheng Basin on the WYK section, bounded by F_1, F_2, and F_3, three branches of the north ZTS fault, respectively.

aeolian sediments (Song et al., 2007, 2014) show small fluctuations of the East Asian summer monsoon. The variations of >19 μm grain-size fraction in aeolian sediments indicate a stable East Asian winter monsoon (An et al., 2001) and a relatively stable deposition rate (Guo et al., 2002).

Drastic climate change and a sharp fall in sea level have taken place since 3.6–3.0 Ma. The Pacific deep water was warmer before ca. 3.5 Ma than at present, but significant cooling and more violent fluctuations corresponded to the formation of the Northern Hemisphere ice sheet during 3.2–2.5 Ma (Tian et al., 2002, 2008). The benthic oxygen isotope record shows that three *super interglacials* occurred between 3.3 and 2.9 Ma (Lisiecki and Raymo, 2005), and during the same period, the magnetic susceptibility of the Chinese Loess rose with fluctuations (Song et al., 2007, 2014; Yang and Ding, 2010). The strengthened summer and winter monsoons in East Asia oscillate strongly, but the enhancement magnitude of the winter monsoon was greater than that of the summer monsoon (An et al., 2001; Sun et al., 2010). Moreover, the deposition rate of aeolian deposits in North China began to increase rapidly at 3.5 Ma (Guo et al., 2002). With the rapid climate deterioration, the global sea level declined sharply and fluctuated with an amplitude of 60–120 m (Miller et al., 2005). Therefore, the climate in North China changed from a stably warm and humid state to a dry and cold state with oscillations.

MAGNETOSTRATIGRAPHY OF THE WYK SECTION

Sedimentary Sequence and Paleomagnetic Sampling

Based on field investigation, this study confirms that the strata on both sides of the WYK River near WYK Village are the most well exposed, with relatively complete and continuous sections (Figs. 3 and 4). The WYK section (35°2′N, 111°10′E, 561 m above sea level [asl]) consists mainly of the Xiaxian Conglomerate overlain by a loess-paleosol sequence. The loess-paleosol layers are comparatively thin, but the S7–S9 (S—paleosol) layers are complete and continuous. The L9 (L—loess), with one weakly developed paleosol in the lower part, is the second thickest layer in the loess-paleosol sequence in North China (Fig. 4I; Liu, 1985; Liu et al., 1988). The same phenomenon has been observed in the Xiaxian section (Xiong et al., 2017). The loess-paleosol layers beneath L9 are much thinner than that above L9, especially the paleosol layers, which are mostly ~0.5 m thick. In total, 13 paleosol layers were distinguished between L9 and the highest conglomerate layer (Fig. 4I). Due to dissection or poor preservation, paleomagnetic sampling of the two paleosol layers beneath S9-1 can't be completed near the ground, although they are clear in the upper part of the section. Therefore, the loess-paleosol sequence below S9-1 are not numbered.

The Xiaxian Conglomerate consists of thick conglomerate layers interbedded with thin sandstone and claystone layers, more than 110 m thick, deposited above the Paleozoic limestone in the east (Fig. 4). The gravels are sub-rounded or sub-angular, and medium-sorted, mixed with red clay blocks. The thickest sandstone layer and conglomerate layer with a large amount of calcium nodules are in the upper part. Taking them as the marker layers, this article links the lower part (Fig. 4A) near the bedrock with the higher part (Fig. 4B) of the Xiaxian Conglomerate near the platform margin. Thin conglomerate, sandstone, and claystone layers are interbedded, and the phenomena that gullies incise claystone layers are obvious above the conglomerate marker layer (Fig. 4G).

The WYK section is divided into 51 stratigraphic horizons with thicknesses of 0.17–19.60 m, each of which has at least one sampling horizon, except for the lowest two conglomerate layers. Paleomagnetic samples were collected at intervals of 0.25 m. Sampling horizons total 220, and every sampling horizon contains three independent samples.

Rock Magnetic Investigation

Magnetic minerals can be distinguished by hysteresis loops and isothermal remanent magnetization acquisition curves (Deng et al., 2004; Xiong et al., 2016b). The frequently used hysteresis loop and magnetic hysteresis parameters are obtained by changing the external magnetic field strength. The saturation magnetization (Ms), saturation isothermal remanent magnetization (Mrs), and coercivity (Bc) are three important parameters of the hysteresis loop. The magnetic field intensity is coercivity of remanence (Bcr) when the remanence is zero after the Mrs-obtained material is placed in a reverse magnetic field. The loess sample shows that the hysteresis loop is close to saturation at ~0.2 T, narrow in the middle, and wider above and below (wasp-waisted style), and Bcr and Bc are close to that of single-domain magnetic minerals (33 and 10 mT, respectively; Figs. 5D and 5H). The behaviors indicate that more low coercivity ferromagnetic minerals and paramagnetic minerals exist (mainly magnetite; Forster and Heller, 1997; Deng et al., 2005). The loess sample shows the same magnetic characteristics as the loess-paleosol sequence of the Xiaxian section (Xiong et al., 2017). The hysteresis loops of samples from sandstone and silty clay layers show a thicker wasp-waist feature closer at ~1.5 T (Figs. 5B and 5C) than that from loess, implying ferromagnetic minerals and more high coercivity minerals (e.g., hematite; Deng et al., 2004; Li et al., 2013). In addition, the sandstone sample also shows that the hysteresis loop is close to saturation at ~0.2 T, but Bcr is higher than the loess sample (Figs. 5A and 5E), which shows that its magnetic minerals content is between the former two types of samples.

The Mrs/Ms and Bcr/Bc ratios of the magnetic minerals can be used to indicate the types of magnetic minerals in the samples (Day et al., 1977). Figure 6 shows that Mrs/Ms and Bcr/Bc ratios of the Xiaxian section deposits and the loess deposits of the WYK section fall mainly within the scope of pseudo-single domain magnetic minerals, and that of the Xiaxian Conglomerate fall mainly within the scope of pseudo-single and single + superparamagnetic domain magnetic minerals. The latter phenomenon can be caused by mixed particles of the same magnetic mineral or mixed magnetic minerals (e.g., magnetite and hematite). The hysteresis loops, isothermal remnant magnetization acquisition curves, and plotted Day diagram indicate that magnetic minerals of loess are mainly magnetite, while magnetic minerals from the Xiaxian Conglomerate in the WYK section are mainly magnetite and a small amount of hematite, which are significantly different magnetic minerals in coercivity.

Demagnetization

In this study, 220 sampling horizons were subjected to thermal demagnetization. Representative demagnetization diagrams of the WYK section are shown in Figure 7. One sample from every sampling horizon of the loess-paleosol strata was subjected to progressive thermal demagnetization up to 590 °C, with a 50 °C interval below 450 °C, a 20 °C interval between 450 and 510 °C, and a 10 °C interval between 510 and 590 °C, using a Magnetic Measurement Thermal Demagnetizer (ASC TD-48). Thermal demagnetization of the Xiaxian Conglomerate was completed by a similar process in which one sample from every sampling horizon was subjected to progressive thermal demagnetization up to 690 °C, with a 50 °C interval below 450 °C, a 40 °C interval between 450 and 570 °C, a 20 °C interval between 570 and 630 °C, and a 10 °C interval between 630 and 690 °C. Once specimens showed unstable demagnetization trajectories, a second round of progressive thermal demagnetization would be selected.

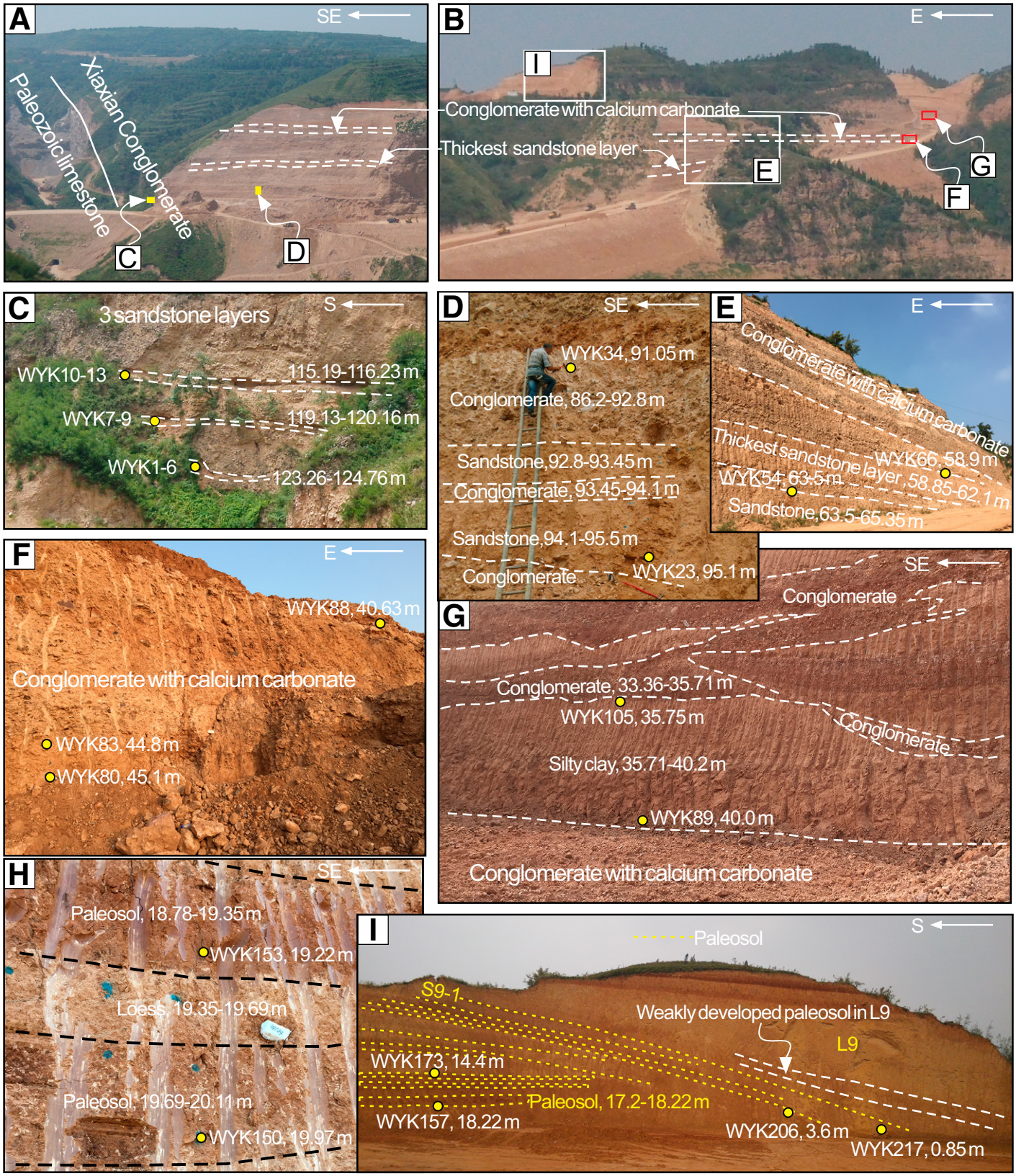

Figure 4. Representative (sampling) photos of the Wangyukou (WYK) section. (A and B) The complete exposures of the section and positions of the segments. (C and D) Conglomerate and sandstone strata in the bottom. (E and F) Conglomerate layer with calcium carbonates and the thickest sandstone layer are two marker layers. (G) Secondary loess interbedded with gravel layer. (H and I) Overlying loess-paleosol sequence with L9, one of the most important marker layers of the loess in North China.

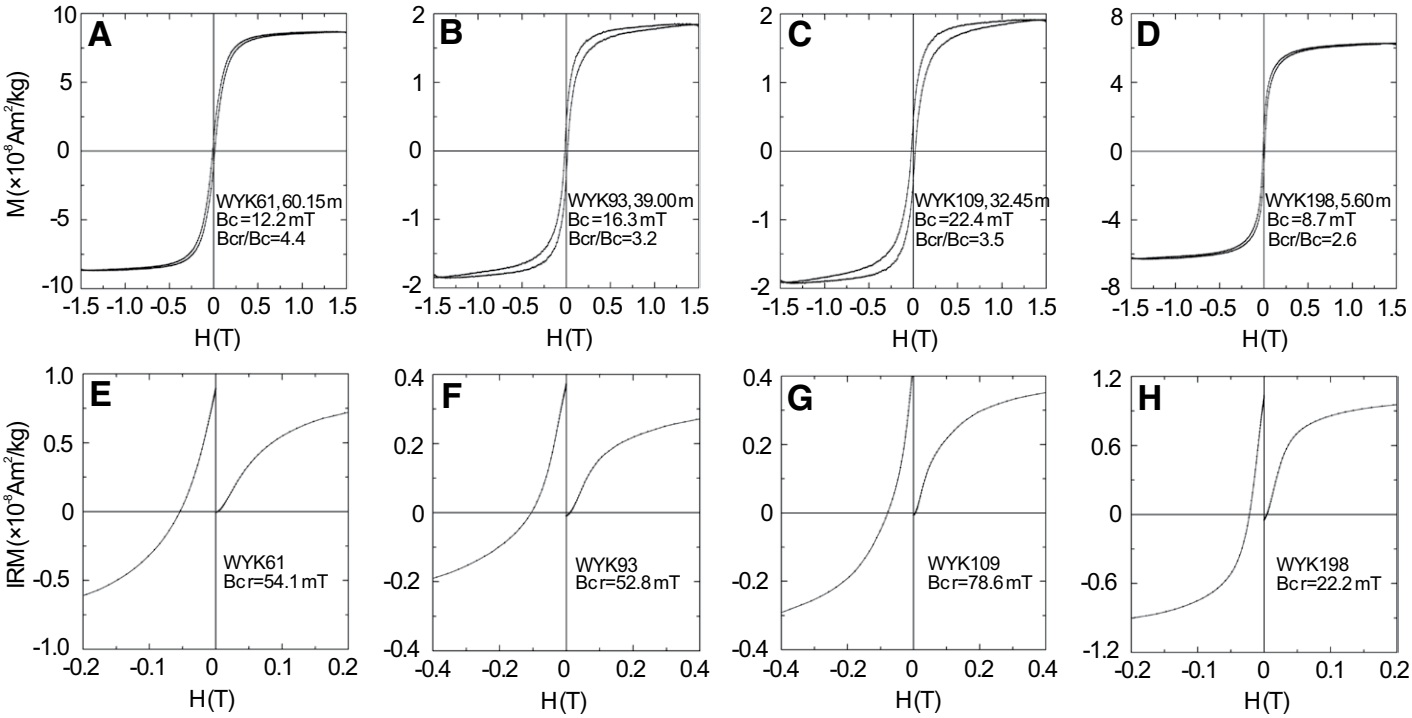

Figure 5. (A–D) Hysteresis loops after slope correction for paramagnetic contribution. (E–H) Isothermal remanent magnetization (IRM) acquisition and back-field demagnetization curves. Samples WYK61 and WYK109 represent the sandstone layers, sample WYK93 represents the silty clay layer of the Xiaxian Conglomerate, and sample WYK198 represents the loess layer above the Xiaxian Conglomerate. M—magnetization; Bc—coercivity; Bcr—coercivity of remanence; H—applied field; WYK—Wangyukou.

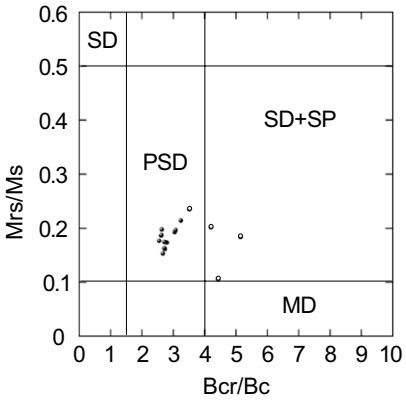

Figure 6. Hysteresis ratios plotted on a Day diagram (Day et al., 1977). Solid circles represent loss sample of the Wangyukou section and loess-paleosol and red clay samples of the Xiaxian section (Xiong et al., 2017); hollow circles represent sandstone and silty clay samples of the Xiaxian Conglomerate. SD—single domain; PSD—pseudo-single domain; MD—multidomain; SP—superparamagnetic; Mrs—saturation isothermal remanent magnetization; Ms—saturation magnetization; Bcr—coercivity of remanence; Bc—coercivity.

The sample remanence was measured by using a 2G cryogenic magnetometer (model 760), which was installed in a magnetically shielded room (<300 nT). The method was capable of separating the characteristic remanent magnetization (ChRM). The principal component directions were computed by the least-squares fitting technique (Kirschvink, 1980). Data from four to five temperature steps above 450 °C or 600 °C trending toward the origin were used for least-squares fits. Samples with a maximum angular deviation >15° were rejected from further analyses. Based on these rules, a total of 133 samples (60.5%; representing 220 sampling horizons) gave reliable ChRM directions of thermal demagnetizations. The magnetic declination and inclination of the samples were then used to calculate virtual geomagnetic pole (VGP) latitudes.

Magnetic Polarity Stratigraphy

Due to some inherent uncertainties of paleomagnetism (Talling and Burbank, 1993), every magnetozone is defined by three samples with VGP latitude ≥45° when constructing the magnetic polarity stratigraphy for the WYK section (Fig. 8A). Magnetozone R1 has two samples with high VGP latitude and two samples with VGP latitude close to 45°; Magnetozone N5 has a similar status, and so they are kept. Due to dissection or poor preservation, it was difficult to distinguish and number the loess/paleosol layers. However, L9, the thickest layer with one weakly developed paleosol in the section, is enough to constrain the top boundary. Consequently, this study takes S9-1 below L9 as the marker layer, and links the WYK section with the Xiaxian section (Xiong et al., 2017).

To summarize, five normal magnetozones (N1 to N5) and five reverse magnetozones (R1 to R5) are identified in the WYK section (Fig. 8A). Every magnetozone is established by three samples at least, two samples of which are from different stratigraphic horizons. The 10 magnetozones in the WYK section are five with reverse polarity: R1 (0–3.48 m), R2 (6.42–18.97 m), R3 (25.86–30.53 m), R4 (61.58–64.13 m), and R5 (94.85–117.52 m); and five with normal polarity: N1 (3.48–6.42 m), N2 (18.97–25.86 m), N3 (30.53–61.58 m), N4 (64.13–95.85 m), and N5 (117.52–124.76 m).

RESULTS

A Span from Late Pliocene to Early Pleistocene of the WYK Section

Paleomagnetic studies of loess in North China have been carried out for more than 40 years, and the paleomagnetic method itself has gradually advanced. The positions of polarity chrons and polarity subchrons in loess-paleosol sequences are more accurate (Heller and Liu,

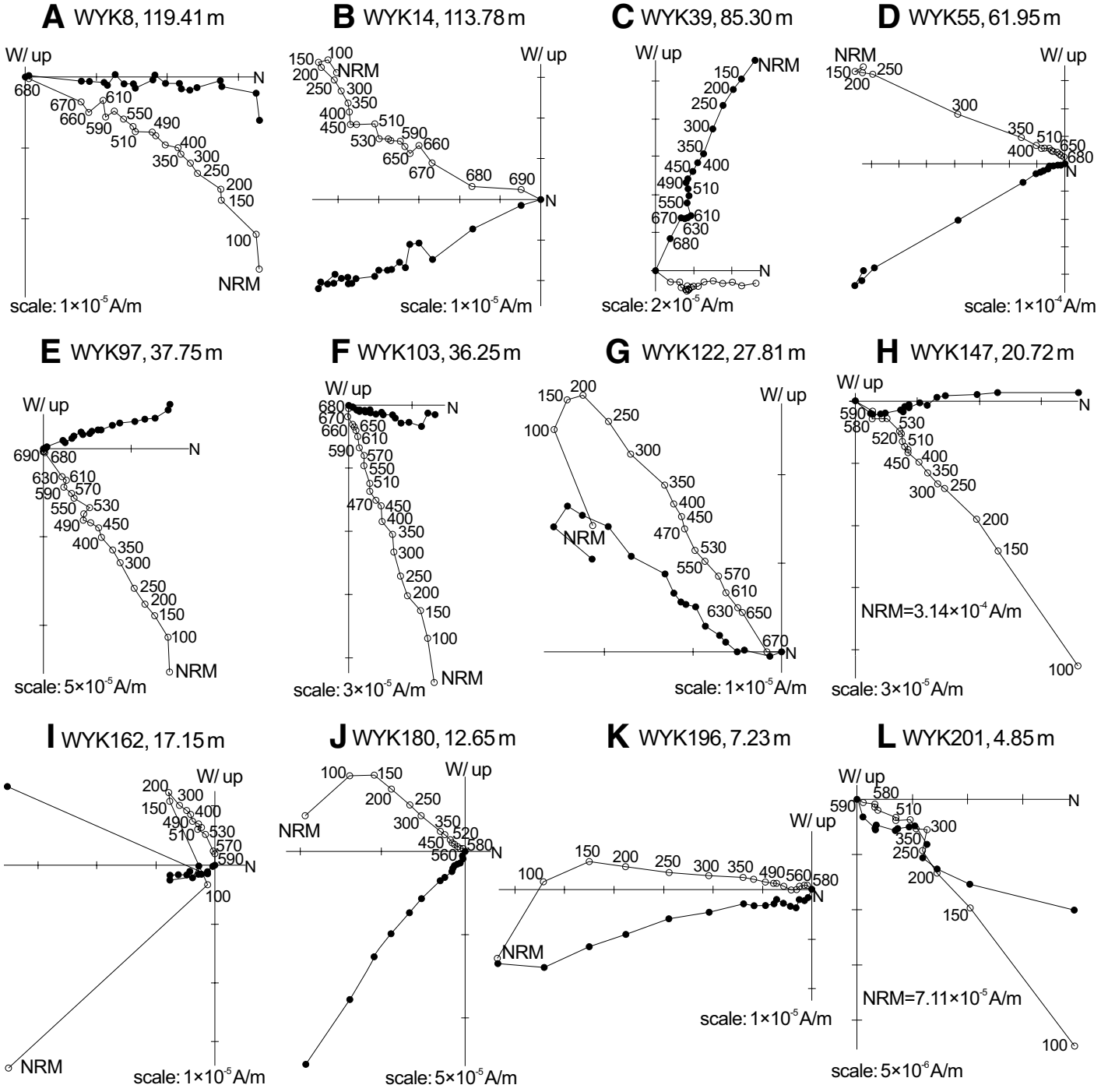

Figure 7. Representative orthogonal plots of the Wangyukou (WYK) section. Samples WYK8, WYK14, WYK39, and WYK55 represent the sandstone layers; samples WYK97, WYK103, and WYK122 represent the silty clay layers of the Xiaxian Conglomerate; and samples WYK147, WYK162, WYK180, WYK196, and WYK201 represent the loess-paleosol sequence above the Xiaxian Conglomerate. The solid (open) circles represent the horizontal (vertical) planes. Thermal treatment levels are marked in °C. NRM—natural remanent magnetization.

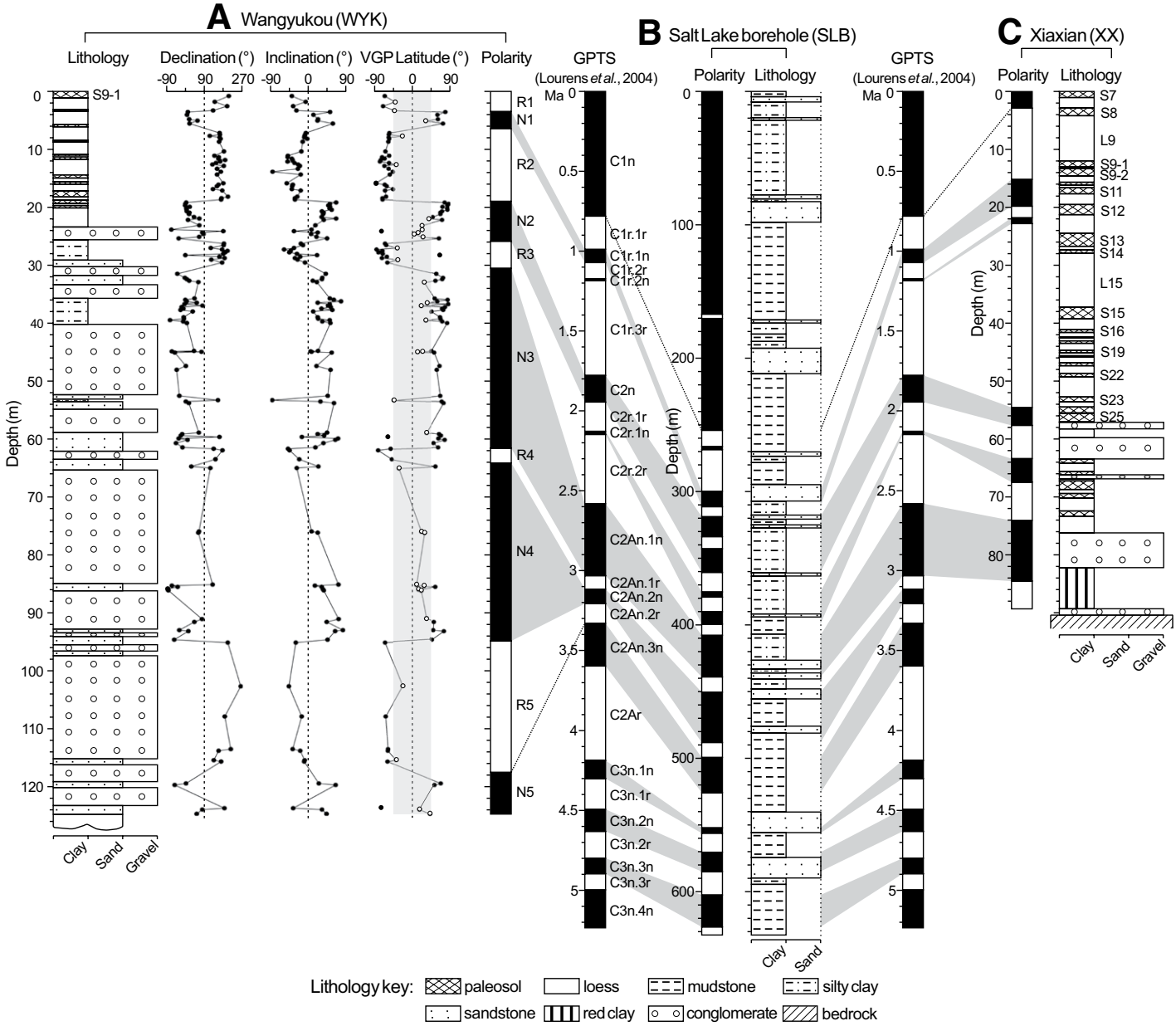

Figure 8. (A) Lithostratigraphy, declination, and inclination of the characteristic remanent magnetization directions, virtual geomagnetic pole (VGP) latitude, and magnetic polarity of the Wangyukou (WYK) section. Open circles represent samples with absolute values of VGPs ≤ 45°, which were not used to define the magnetic polarity stratigraphy (except for R1 and N5; please see the article for details). Boundaries between magnetozones are defined by the midpoint between two samples with opposite polarity. Lithostratigraphy with rectangle's length representing grain size of the sedimentary. GPTS—geomagnetic polarity timescale (Lourens et al., 2004). (B and C) Lithostratigraphy and magnetic polarity stratigraphy of the Salt Lake borehole (Wang et al., 2002), and Xiaxian (Xiong et al., 2017) sections. S—paleosol; L—loess.

1984, 1986). Although the hysteresis effect of remanent magnetization acquisition, the remagnetization phenomenon, rapid polarity swings (Yang et al., 2004, 2008, 2010), and different judgments of the boundary between loess and paleosol may exist, the specific positions of the polarity chrons and subchrons in the geomagnetic polarity timescale (GPTS) are basically certain. L9, S9-1, and S9-2 are all in the subchron C1r.1r (Liu et al., 1988; Wang et al., 2010); the top and bottom boundaries of the Jaramillo (C1r.1n) are in the middle of L10 and at the bottom of L12, respectively (Yang et al., 2004; Xiong et al., 2017); the Olduvai subchron (C2n) is from the top of S24 to the top of S26 (Yang et al., 2007; Xiong et al., 2017); the Matuyama/Gauss boundary is in the upper part of the lowest loess layer (Yang et al., 2007; Xiong et al., 2017).

Beneath L9 are 24 paleosol layers in the loess-paleosol sequence in North China (Yang and Ding, 2010; Xiong et al., 2017). There are only 13 paleosol layers below L9, so 11 paleosol layers are missing beneath L9 in the WYK section (Figs. 4I and 8A). Paleomagnetic samples have not been collected in two paleosol layers because they are dissected by one loess layer below S9-1. The magnetostratigraphy indicates two normal magnetozones in the loess-paleosol sequence of the section, of which one is from the second loess layer within the third paleosol, and

the other is at the bottom of the loess-paleosol sequence within the first conglomerate layer. Consequently, compared with the Xiaxian section (Xiong et al., 2017), N1 and N2 are considered as the Jaramillo and Olduvai subchrons, respectively. Between L9 and S24, the first layer of the Olduvai subchron in the Xiaxian section, 16 paleosol layers are identified (Xiong et al., 2017), so five paleosol layers are missing at the same place of the WYK section (Fig. 8A). Meanwhile, the Cobb Mountain subchron (C1r.2n) and Reunion subchron (C2r.1n) are not found in the magnetostratigraphy because of comparatively thin layers and short-term subchrons, which is very normal in North China (Hu et al., 2012; Pan et al., 2012). The magnetozones of N3–N5 correspond to C2An.1n–C2An.3n one by one. Based on these comparisons, this study deems that the WYK section is constrained to a span from the late Pliocene to early Pleistocene and that the Xiaxian Conglomerate is constrained to a span in the late Pliocene. The magnetostratigraphy is consistent with 1:200,000 Chinese geologic maps (Ministry of Geology and Mineral Resources) and analogous to the stratigraphy research (Wang et al., 1996).

The Revised Formation Age of the TXPS

The Miocene–Pliocene aeolian red clays are widely distributed in the Ordos Block and Shanxi Graben System (Li et al., 1998; Zhu et al., 2008; Hu et al., 2016). The TXPS in northwestern ZTS is covered by a late Pliocene red clay sequence with varying thickness (Xiong et al., 2017). These indicate that the red clays kept depositing during the Pliocene. However, it couldn't be preserved, and it was transported and accumulated in the piedmont and Yuncheng Basin due to pedimentation. The middle and lower part of the Xiaxian Conglomerate containing a large number of lump or granular red clays should be the correlative sediments of the pedimentation process (Figs. 4B–4D). The red clays have been preserved but partly suffered subsequent river erosion and dissection since the pedimentation was terminated, which has led to the differences in sedimentary sequence overlying it (Xiong et al., 2017).

The accumulation rate of the Xiaxian Conglomerate was abnormally high before 3.1 Ma but began to decrease dramatically at ca. 3.1 Ma (Fig. 9). Since 3.1 Ma, the Xiaxian Conglomerate had finer sediments than before and showed the clay emergence (Fig. 8A). Moreover, the Yuncheng Basin had a high deposition rate at 3.6–3.1 Ma (Fig. 10), although it's unclear whether tectonic activity or climate change was the cause. In any case, 3.1 Ma became an important demarcation point. Therefore, this article revises the final formation age of the TXPS to ca. 3.1 Ma. Prior to it, the pedimentation was in steady progress, and the amount of transported material was relatively stable for the Xiaxian Conglomerate and Yuncheng Basin. After this time, pedimentation was replaced by dissection, and the rivers were unable to erode and transport more sediments; thus, supplies decreased. At 2.6 Ma, the large-scale conglomerate and sandstone aggradation was replaced by secondary loess interbedded with a gravel layer (Fig. 4G). Only the loess-paleosol sequence has deposited since ca. 1.9 Ma, indicating that streams kept trenching with no more gravels and sands depositing (Figs. 4H, 4I, and 8A). The latter two stages can also be observed in the Xiaxian section (Xiong et al., 2017).

DISCUSSION

Steady Activity of the North Zhongtiao Shan Fault—An Important Basis for Planation

The edge of the Xiaxian Platform with the TXPS and Xiaxian Conglomerate is more than 300 m above the basin (Figs. 3 and 4A), and the north ZTS fault controls this. Through comparisons between magnetozone elevation of the WYK section and Salt Lake borehole section (Table 1), this research found that the height difference of each magnetozone before 2.6 Ma is coincidently ~700 m. But this difference

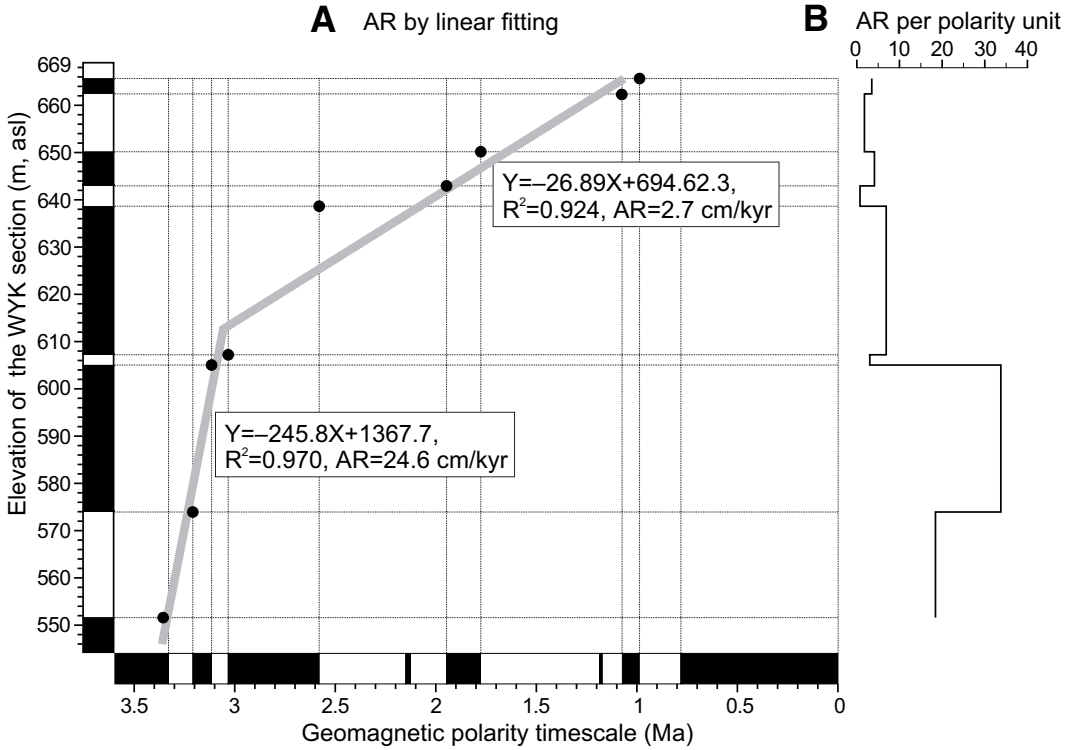

Figure 9. Accumulation rates of the Wangyukou (WYK) section by linear fitting (A) and at per polarity unit (B). AR—accumulation rate; asl—above sea level.

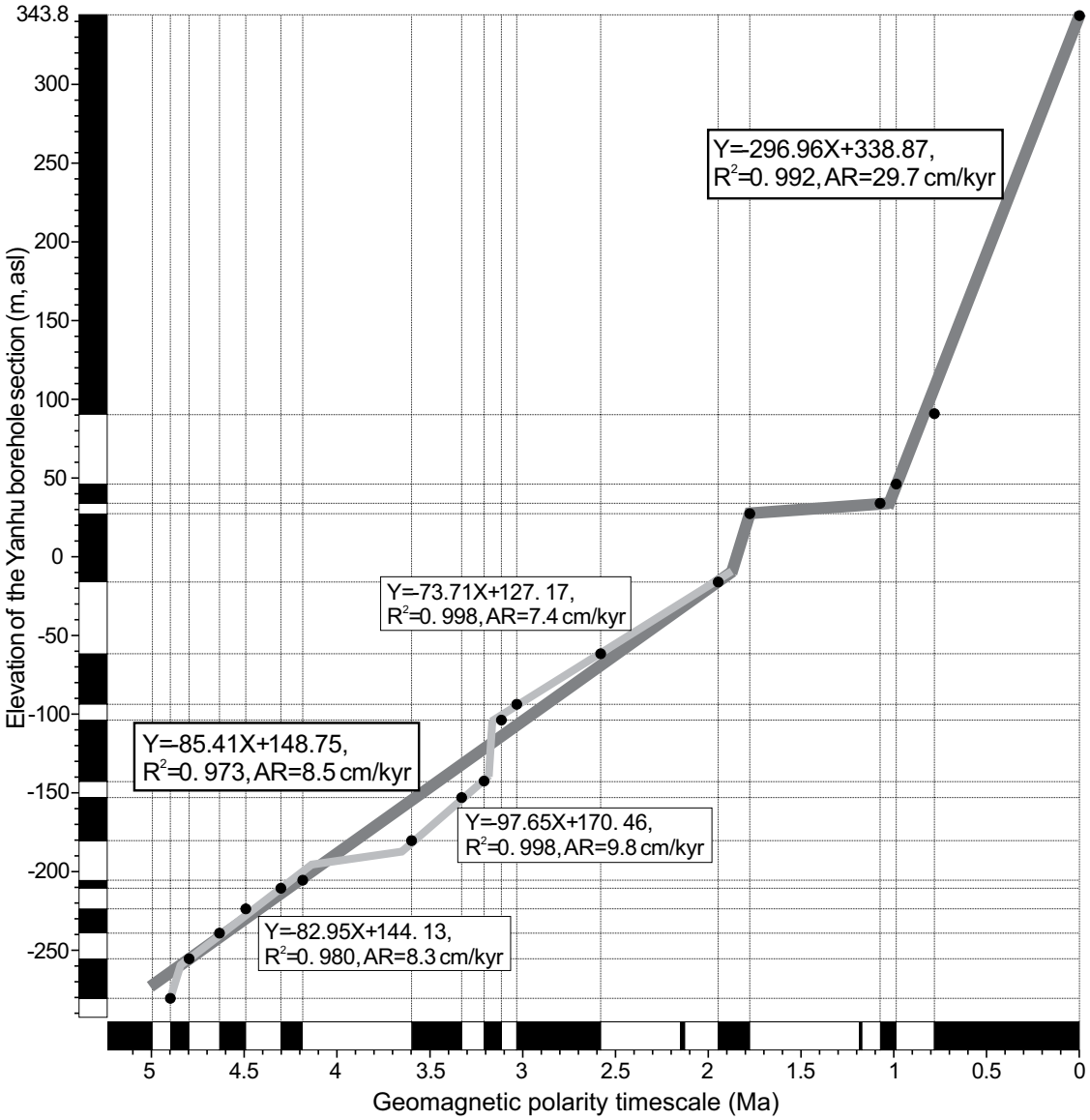

Figure 10. Accumulation rates of the Salt Lake borehole section by linear fitting. The Yuncheng Basin showed a steady accumulation rate before ca. 1.9 Ma, a fluctuation rate between ca. 1.9 Ma–1.0 Ma, and an accelerated rate after ca. 1.0 Ma. Magnetostratigraphy data are from Wang et al. (2002). AR—accumulation rate; asl—above sea level.

TABLE 1. ELEVATION DIFFERENCES BETWEEN THE MAGNETOZONES OF THE MAGNETOSTRATIGRAPHIES OF THE WANGYUKOU SECTION AND SALT LAKE BOREHOLE SECTION IN THE YUNCHENG BASIN

Magnetozone	Terminal age (Ma)*	Elevation of top boundary in the SLB section (m)†	Elevation of top boundary in the WYK section (m)†	Elevation difference (m)
C1r.1n (Jaramillo)	0.988	45.2	665.5	620.3
C1r.2r	1.072	33.4	662.6	629.2
C2n (Olduvai)	1.778	26.4	650.0	623.6
C2r.1r	1.945	–16.6	643.2	659.8
C2An.1n (Gauss)	2.581	–62.6	638.5	701.1
C2An.1r (Keana)	3.032	–94.3	607.4	701.7
C2An.2n	3.116	–104.7	604.9	709.6
C2An.2r (Mammoth)	3.207	–143.4	574.2	717.6
C2An.3n (Gauss)	3.33	–153.7	551.5	705.2

Note: SLB—Salt Lake borehole; WYK—Wangyukou.
*Terminal age of each magnetozone is from the geomagnetic polarity timescale (Lourens et al., 2004).
†Thickness data are converted to elevations above sea level, and the magnetostratigraphy of the Salt Lake borehole section is from Wang et al. (2002).

decreases gradually in the magnetozones of the Pleistocene, because of the low rate of loess deposition due to increased slope gradients near the margin of the uplifted Xiaxian Platform, which was caused by fault F_2 activities (Figs. 3B and 3C). The sedimentary facies change and deposition rate decrease suggest that fault F_2 has been active, while fault F_1 has been inactive since ca. 2.6 Ma, which led to the uplift of the Xiaxian Conglomerate and the TXPS with the overlying sediments to form the Xiaxian Platform.

During the planation process, the elevation of the TXPS was definitely similar or close to that of the basin accumulation surface as the base level, otherwise fluvial dissection would have led to planation termination. The stable conglomerate accumulation ended in the Xiaxian Conglomerate at ca. 2.6 Ma, when the conglomerate surface should have been close to the basin surface. The vertical rates of the north ZTS fault have been 0.25 mm/a since 3.1 Ma and 0.27 mm/a since 2.6 Ma, constrained by comparing the TXPS and Xiaxian Conglomerate surface with the corresponding accumulation surface of the Salt Lake borehole (Table 2). Moreover, the deposition rate and sedimentary facies of the Yuncheng basin were also comparatively stable during the Pliocene and early Pleistocene (Fig. 10). Additionally, during the Cenozoic the Ordos Block was stable (Bao et al., 2013; Hu et al., 2016). Therefore, the vertical rate of the north ZTS fault has been steady, leading to the steady separation between the ZTS and Yuncheng Basin since the Pliocene. The base level, i.e., the Yuncheng Basin surface, was relatively steady.

Based on this analysis, the ZTS and Yuncheng Basin showed no signs of accelerated separation during the Pliocene–early Pleistocene, although accelerated activities existed in other areas. Stable tectonic activity, i.e., the long-term stable vertical rate of the north ZTS fault, is an important basis for planation (Coltorti et al., 2007; Wu, 2008).

TABLE 2. VERTICAL RATE OF THE NORTH ZHONGTIAO SHAN FAULT IN LATE CENOZOIC CONSTRAINED BY GEOMORPHIC SURFACES

Geomorphic surface	Age (Ma)	Elevation (m)	Elevation of corresponding sedimentation surface in SLB section (m)*	Elevation difference (m)	Vertical rate (mm/a)
Tangxian planation surface	3.12	680†	–104.7	784.7	0.25
Xiaxian Conglomerate surface	2.58	638.5§	–62.6	701.1	0.27

Note: SLB—Salt Lake borehole.
*Thickness data are converted to elevations above sea level, and the magnetostratigraphy of the Salt Lake borehole section is from Wang et al. (2002).
†The bedrock surface on the edge of the Xiaxian Platform represents the Tangxian planation surface (Xiong et al., 2017).
§The figure is the conglomerate surface elevation on the edge of the Xiaxian Conglomerate.

Drastic Climate Change Might Have Driven the Tangxian Planation Surface Formation

Climate change will affect the slope processes relative to the four distinct elements of a single hillside (King, 1953). East Asia was stably warm-humid with small fluctuation monsoons from the late Miocene to early Pliocene (Fig. 11), maintaining a high global sea level (Miller et al., 2005). Wu (2008) considered that the planation epoch lasted 2–3 Ma. Therefore, the stably warm-humid climate was another important base for planation. Pediments are the most efficiently developed at semiarid areas due to efficient transport of waste from the free faces and debris slopes (King, 1953). However, the TXPSs were widely developed in warm-humid North China (Fig. 2), seemingly challenging the previous cognition. More rainfall brings increased discharge, and intense incisions occur with difficulty during pedimentation. So debris will be more efficiently transported across the pediment in a humid area than in arid/semiarid area, and stable slope retreat promotes pediment development. Erosion and deposition, both influenced by climate change and tectonic uplift, reach a dynamic balance.

The deposition rate of the Yuncheng Basin was slightly higher during 3.6–3.1 Ma (Fig. 10), possibly caused by tectonic uplift. However, the great changes of the East Asian climate system since the late Pliocene (Fig. 11) might have ended the denudation in the planation surface development process and driven the beginning of accumulation overlying on the TXPS. When the climate was cold and dry, the weakened stream dynamics would lead to debris accumulation that could protect the free faces and debris slopes from being eroded. When the climate would turn warm and humid, increased discharge and vegetation would weaken slope erosion and reduce sediments to enhance stream power; consequently, the streams would have cut through the loose sediments accumulated during the cold period. During one or several climate cycles, due to the separation between the planation surface and basin surface as the base level, bedrocks would have been eroded and dissected. The absence of free faces and the protection of the debris slopes mean that the planation surface development by parallel retreat would have been hindered or aborted (Wood, 1942; King, 1953). The switch from one erosive state to another may make erosion more rapid than if one is left to do all of the erosive work (Zhang et al., 2001). In the background of moderate tectonic activities, fluvial dissection caused by climate change or eustasy is capable of resulting in the separation between the base level and planation surface. This is a possible mechanism for the planation surface disintegration, similar to climate change influencing terrace formation (Starkel, 2003; Stinchcomb et al., 2012). Previous studies have indicated that the TXPS in North China was formed in the late Pliocene (Fig. 11G; Deng et al., 2008; Liu et al., 2016; Pan et al., 2012). Therefore, compared with moderate tectonic uplift, climate with frequent, high-amplitude variations and rapidly declining sea level is more likely to have been the main driver of the final formation and disintegration of the TXPS.

When pedimentation was terminated, the TXPS became the Xiaxian Platform due to tectonic uplift. Aeolian deposits can be preserved on the TXPS, but fluvial processes might erode some deposits (Xiong, et, al., 2017). The Xiaxian Platform rose to a certain height at ca. 1.9 Ma; accordingly, the retrogressive erosion and incising of gullies caused the conglomerate accumulation to be replaced by the complete aeolian loess-paleosol sequence (Figs. 8A and 8C). In the late Pliocene, drastic climate change triggered the planation end and initial covering. Then, dissection of the surface and its burial by conglomerates and aeolian deposits were jointly influenced by tectonic uplift and climate change.

No fast uplift events younger than 8 Ma have been found in the Ordos Block and around the Shanxi Graben System (Chen et al., 2012; Liu et al., 2013; Cao et al., 2015). The Ordos Block was stable during the late Miocene to early Pliocene; the rapid downward cutting of fluvial systems indicates enhanced tectonic uplift since 1.2 Ma (Pan et al., 2012; Bao et al., 2013; Hu et al., 2017). The present global positioning system velocity field in North China is at a lower level (Wang et al., 2001). Although the activity history of each fault is unknown, it seems that this area was stable in the late Miocene to early Pliocene, and it is the most important condition of the planation surface development (Dohrenwend, 1994). Furthermore, the TXPSs are widely distributed in almost all of the mountains in North China (Figs. 1B and 2). Therefore, the unified formation age of the TXPSs (Wu, 2008), and the example of the ZTS, encourage us to consider that drastic climate change may have been the

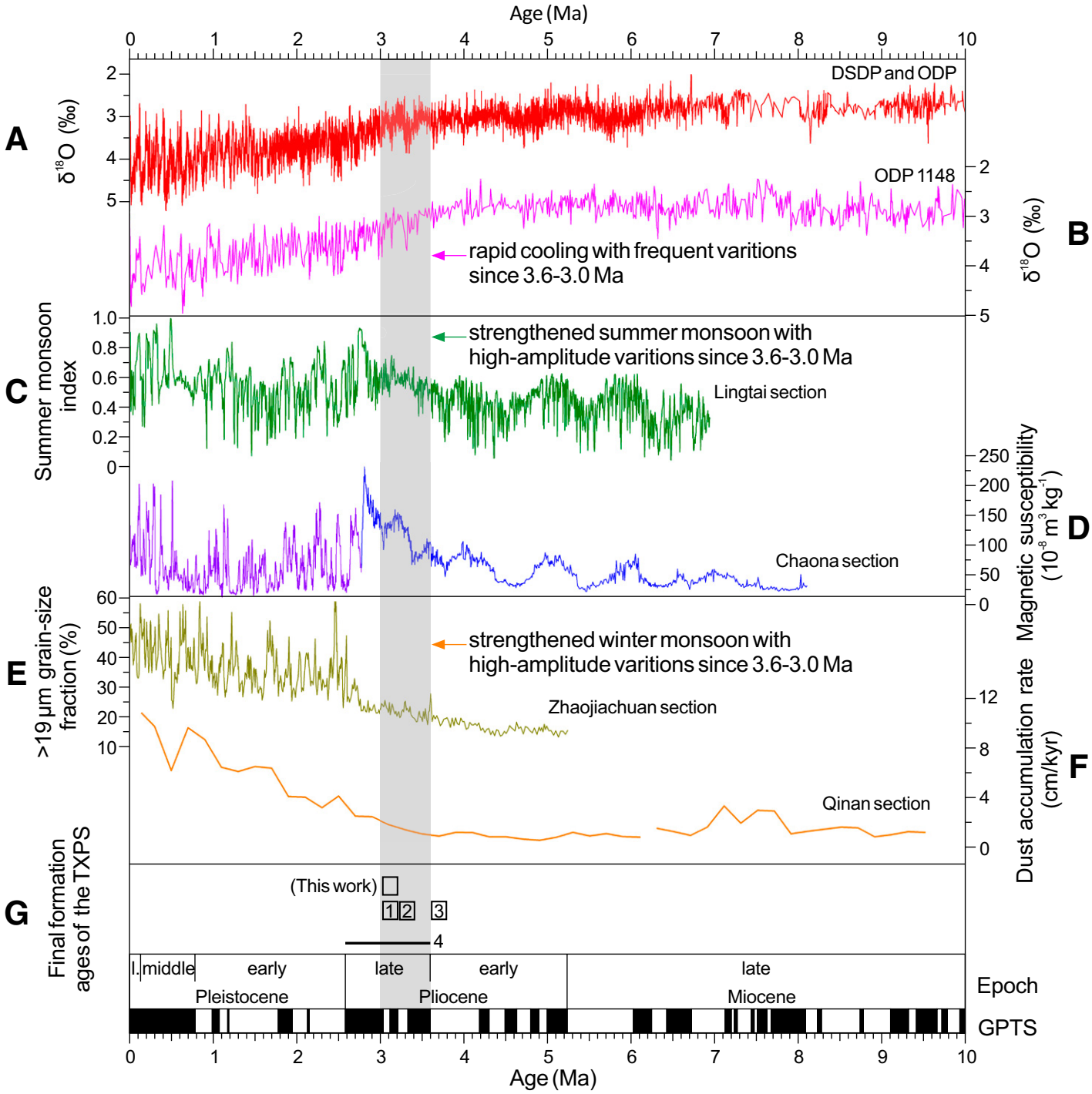

Figure 11. Records of climate change since 10 Ma. (A) Stacked deep-sea benthic foraminiferal oxygen-isotope curve based on records from more than 40 Deep Sea Drilling Project (DSDP) and Ocean Drilling Program (ODP) sites (Zachos et al., 2001). (B) Benthic foraminiferal oxygen-isotope curve based on records from ODP Site 1148 in the South China Sea (Tian et al., 2008). (C) Summer monsoon index based on magnetic susceptibility and carbonate content of the Lingtai section (Sun et al., 2010). (D) Magnetic susceptibility before (Song et al., 2014) and after (Song et al., 2007) 2.77 Ma of the Chaona section. (E) >19 μm grain-size fraction from the Zhaojiachuan section (An et al., 2001). (F) Dust accumulation rate of the Qinan section (Guo et al., 2002). (G) Final formation ages of the Tangxian planation surface in North China. 1—Nihewan area in the north Shanxi Graben System (Deng et al., 2008); 2 and 3—Wubao (Liu et al., 2016) and Xing (Pan et al., 2012) areas in the Ordos Block; 4—summary of the planation surface formation age in North China (Wu, 2008). GPTS—geomagnetic polarity timescale (Lourens et al., 2004).

main driving force of the final formation of the TXPS in North China.

CONCLUSIONS

The WYK section in the northwest ZTS of the Shanxi Graben System in North China, related to the TXPS development, was studied. A high-resolution magnetostratigraphy constrained the deposition era of the section to a span from the late Pliocene to early Pleistocene. Based on the deposition rate, sedimentary facies changes, and sediment characteristics of the WYK section and Salt Lake borehole section in the Yuncheng Basin, the final formation age of the TXPS has been revised to be 3.1 Ma. The vertical rates of the north ZTS fault have been 0.25 mm/a since 3.1 Ma and 0.27 mm/a since 2.6 Ma, constrained by comparing the TXPS and Xiaxian Conglomerate surface with the corresponding accumulation surface of the Salt Lake borehole, which indicate stable tectonic activities. The climate in North China was stably warm-humid from the late Miocene to early Pliocene. They are both important bases for pediment development. However, abrupt climatic changes during the late Pliocene might have been the main driving force of the final formation of the TXPS.

ACKNOWLEDGMENTS

Rock magnetic investigations and demagnetization were made in the Paleomagnetism and Geochronology Laboratory, Institute of Geology and Geophysics, Chinese Academy of Sciences. This research was jointly financed by the National Natural Science Foundation of China (Grants 41271019, 41590861, 41702219, and 41661134011), the China Postdoctoral Science Foundation (Grant 2017M622854), the Minle-Damaying Active Fault special scientific research of earthquake industry in China (Grant 201408023), and the Guangdong Province Introduced Innovative R&D Team of Geological Processes and Natural Disasters around the South China Sea (2016ZT06N331). Professors Michael Oskin, Yang Jingchun, Wu Chen, Li Dewen, Xia Zhengkai, Mo Duowen, Liu Gengnian, Zhang Jiafu, Zhang Shimin, and He Honglin and Dr. Li Shihu, Katherine Schide, and Erica Danielle Erlanger are highly appreciated for their very constructive comments on this manuscript. Mr. Xue Jisuo and Mr. Hou Wenqiang are thanked for their field assistance. Professor Johan Bonow, three anonymous reviewers, and the editor, Professor Kurt Stuewe, are especially thanked for their careful reading, constructive comments, and language improvements.

REFERENCES CITED

Adams, G., 1975, Planation Surfaces: Stroudsburg, Pennsylvania, Dowden, Hutchinson & Ross, Inc., Halsted Press, 492 p.

An, Z., Kutzbach, J.E., Prell, W.L., and Porter, S.C., 2001, Evolution of Asian monsoons and phased uplift of the Himalaya–Tibetan plateau since Late Miocene times: Nature, v. 411, no. 6833, p. 62–66, https://doi.org/10.1038/35075035.

Bao, X., Song, X., Xu, M., Wang, L., Sun, X., Mi, N., Yu, D., and Li, H., 2013, Crust and upper mantle structure of the North China Craton and the NE Tibetan Plateau and its tectonic implications: Earth and Planetary Science Letters, v. 369, p. 129–137, https://doi.org/10.1016/j.epsl.2013.03.015.

Cao, X., Li, S., Xu, L., Guo, L., Liu, L., Zhao, S., Liu, X., and Dai, L., 2015, Mesozoic–Cenozoic evolution and mechanism of tectonic geomorphology in the central North China Block: Constraint from apatite fission track thermochronology: Journal of Asian Earth Sciences, v. 114, p. 41–53, https://doi.org/10.1016/j.jseaes.2015.03.041.

Casas-Sainz, A.M., and Cortés-Gracia, A.L., 2002, Cenozoic landscape development within the central Iberian Chain, Spain: Geomorphology, v. 44, no. 1, p. 19–46, https://doi.org/10.1016/S0169-555X(01)00129-5.

Chen, F., Yu, Z., Yang, M., Ito, E., Wang, S., Madsen, D.B., Huang, X., Zhao, Y., Sato, T., Birks, H.J.B., Boomer, I., Chen, J., An, C., and Wünnemann, B., 2008, Holocene moisture evolution in arid central Asia and its out-of-phase relationship with Asian monsoon history: Quaternary Science Reviews, v. 27, no. 3–4, p. 351–364, https://doi.org/10.1016/j.quascirev.2007.10.017.

Chen, G., Ding, C., Xu, L., Zhang, H., Hu, Y., Yang, F., Li, N., and Mao, X., 2012, Analysis on the thermal history and uplift process of Zijinshan intrusive complex in the eastern Ordos basin: Chinese Journal of Geophysics, v. 56, no. 1, p. 78–90, https://doi.org/10.1002/cjg2.20007.

Cheng, S., Deng, Q., Zhou, S., and Yang, G., 2002, Strath terraces of Jinshaan Canyon, Yellow River, and Quaternary tectonic movements of the Ordos Plateau, North China: Terra Nova, v. 14, no. 4, p. 215–224, https://doi.org/10.1046/j.1365-3121.2002.00350.x.

Coltorti, M., and Pieruccini, P., 2000, Late Lower Pliocene planation surface across the Italian Peninsula: A key tool in neotectonic studies: Journal of Geodynamics, v. 29, no. 3, p. 323–328, https://doi.org/10.1016/S0264-3707(99)00049-6.

Coltorti, M., Dramis, F., and Ollier, C.D., 2007, Planation surfaces in northern Ethiopia: Geomorphology, v. 89, no. 3, p. 287–296, https://doi.org/10.1016/j.geomorph.2006.12.007.

Cui, Z., Li, D., Wu, Y., and Liu, G., 1999, Comment on planation surface: Chinese Science Bulletin, v. 44, no. 22, p. 2017–2022, https://doi.org/10.1007/BF02884913.

Day, R., Fuller, M., and Schmidt, V.A., 1977, Hysteresis properties of titanomagnetites: Grain size and compositional dependence: Physics of the Earth and Planetary Interiors, v. 13, no. 4, p. 260–267, https://doi.org/10.1016/0031-9201(77)90108-X.

Deng, C., Zhu, R., Verosub, K.L., Singer, M.J., and Vidic, N.J., 2004, Mineral magnetic properties of loess/paleosol couplets of the central loess plateau of China over the last 1.2 Myr: Journal of Geophysical Research, D, Atmospheres, v. 109, p. B01103, https://doi.org/10.1029/2003JB002532.

Deng, C., Vidic, N.J., Verosub, K.L., Singer, M.J., Liu, Q., Shaw, J., and Zhu, R.X., 2005, Mineral magnetic variation of the Jiaodao Chinese loess/paleosol sequence and its bearing on long-term climatic variability: Journal of Geophysical Research, D, Atmospheres, v. 110, B3, p. 767–782, https://doi.org/10.1029/2004JB003451.

Deng, C., Zhu, R., Zhang, R., Ao, H., and Pan, Y., 2008, Timing of the Nihewan formation and faunas: Quaternary Research, v. 69, p. 77–90, https://doi.org/10.1016/j.yqres.2007.10.006.

Deng, Q., Ran, Y., Yang, X., Min, W., and Chu, Q., 2007, Map of Active Tectonics of China: China, Seismology Press, scale 1:4,000,000.

Dohrenwend, J.C., 1994, Pediments in Arid Environments, *in* Abrahams, A.D., and Parsons, A.J., eds., Geomorphology of Desert Environments: London, Chapman and Hall, p. 321–353, https://doi.org/10.1007/978-94-015-8254-4_13.

Evenstar, L.A., Hartley, A.J., Stuart, F.M., Mather, A.E., Rice, C.M., and Chong, G., 2009, Multiphase development of the Atacama Planation Surface recorded by cosmogenic ^{3}He exposure ages: Implications for uplift and Cenozoic climate change in western South America: Geology, v. 37, no. 1, p. 27–30, https://doi.org/10.1130/G25437A.1.

Forster, T., and Heller, F., 1997, Magnetic enhancement paths in loess sediments from Tajikistan, China and Hungary: Geophysical Research Letters, v. 24, p. 17–20, https://doi.org/10.1029/96GL03751.

Goudie, A.S., 2004, Encyclopedia of geomorphology: New York, Routledge, p. 768–770, 788–792.

Guo, Z.T., Ruddiman, W.F., Hao, Q.Z., Wu, H.B., Qiao, Y.S., Zhu, R.X., Peng, S.Z., Wei, J.J., Yuan, B.Y., and Liu, T.S., 2002, Onset of Asian desertification by 22 Myr ago inferred from loess deposits in China: Nature, v. 416, no. 6877, p. 159–163, https://doi.org/10.1038/416159a.

Heller, F., and Liu, T., 1984, Magnetism of Chinese loess deposits: Geophysical Journal International, v. 77, no. 1, p. 125–141, https://doi.org/10.1111/j.1365-246X.1984.tb01928.x.

Heller, F., and Liu, T., 1986, Palaeoclimatic and sedimentary history from magnetic susceptibility of loess in China: Geophysical Research Letters, v. 13, no. 11, p. 1169–1172, https://doi.org/10.1029/GL013i011p01169.

Hu, Z., Pan, B., Wang, J., Cao, B., and Gao, H., 2012, Fluvial terrace formation in the eastern Fenwei Basin, China, during the past 1.2 Ma as a combined archive of tectonics and climate change: Journal of Asian Earth Sciences, v. 60, p. 235–245, https://doi.org/10.1016/j.jseaes.2012.09.016.

Hu, Z., Pan, B., Guo, L., Vandenberghe, J., Liu, X., Wang, J., Fan, Y., Mao, J., Gao, H., and Hu, X., 2016, Rapid fluvial incision and headward erosion by the Yellow River along the Jinshaan gorge during the past 1.2 Ma as a result of tectonic extension: Quaternary Science Reviews, v. 133, p. 1–14, https://doi.org/10.1016/j.quascirev.2015.12.003.

Hu, Z., Pan, B., Bridgland, D., Vandenberghe, J., Guo, L., Fan, Y., and Westaway, R., 2017, The linking of the upper-middle and lower reaches of the Yellow River as a result of fluvial entrenchment: Quaternary Science Reviews, v. 166, p. 324–338, https://doi.org/10.1016/j.quascirev.2017.02.026.

King, L.C., 1953, Canons of landscape evolution: Geological Society of America Bulletin, v. 64, no. 7, p. 721–752, https://doi.org/10.1130/0016-7606(1953)64[721:COLE]2.0.CO;2.

Kirschvink, J.L., 1980, The least-squares line and plane and the analysis of palaeomagnetic data: Geophysical Journal of the Royal Astronomical Society, v. 62, no. 3, p. 699–718, https://doi.org/10.1111/j.1365-246X.1980.tb02601.x.

Li, S., Deng, C., Yao, H., Huang, S., Liu, C., He, H., Pan, Y., and Zhu, R., 2013, Magnetostratigraphy of the Dali Basin in Yunnan and implications for late Neogene rotation of the southeast margin of the Tibetan Plateau: Journal of Geophysical Research, D, Atmospheres, v. 118, p. 791–807, https://doi.org/10.1002/jgrb.50129.

Li, Y., Yang, J., Xia, Z., and Mo, D., 1998, Tectonic geomorphology in the Shanxi Graben System, northern China: Geomorphology, v. 23, no. 1, p. 77–89, https://doi.org/10.1016/S0169-555X(97)00092-5.

Lin, A., Rao, G., and Yan, B., 2015, Flexural fold structures and active faults in the northern–western Weihe Graben, central China: Journal of Asian Earth Sciences, v. 114, p. 226–241, https://doi.org/10.1016/j.jseaes.2015.04.012.

Lisiecki, L.E., and Raymo, M.E., 2005, A Pliocene-Pleistocene stack of 57 globally distributed benthic δ^{18}O records: Paleoceanography, v. 20, PA1003, https://doi.org/10.1029/2004PA001071.

Liu, J., Zhang, P., Lease, R.O., Zheng, D., Wan, J., Wang, W., and Zhang, H., 2013, Eocene onset and late Miocene acceleration of Cenozoic intracontinental extension in the North Qinling range–Weihe graben: Insights from apatite fission track thermochronology: Tectonophysics, v. 584, p. 281–296, https://doi.org/10.1016/j.tecto.2012.01.025.

Liu, T.S., 1985, Loess and Environment: Beijing, Science Press, p. 48–61 (in Chinese).

Liu, X., Liu, T., Xu, T., Liu, C., and Chen, M., 1988, The Chinese loess in Xifeng, I. The primary study on magnetostratigraphy of a loess profile in Xifeng area, Gansu province: Geophysical Journal International, v. 92, no. 2, p. 345–348, https://doi.org/10.1111/j.1365-246X.1988.tb01146.x.

Liu, Y., Li, Y., and Zhou, B., 2016, Terrace sequences and their formation ages in Pantang-Heiyukou area, Northern Shanxi-Shaanxi Gorge, China [in Chinese with English abstract]: Beijing Da Xue Xue Bao, Zi Ran Ke Xue Bao, v. 52, no. 2, p. 257–264, https://doi.org/10.13209/j.0479-8023.2015.139.

Lourens, L., Hilgen, F., Shackleton, N.J., Laskar, J., and Wilson, D., 2004. The Neogene Period, *in* Gradstein, F.M., Ogg, J.G, and Smith, A.G., eds., A Geologic Time Scale: Cambridge, Cambridge University Press, p. 409–440.

Lv, S.H., Li, Y.L., Wang, Y.R., and Ci, H.J., 2014, The Holocene paleoseismicity of the north Zhongtiao Shan faults in Shanxi Province, China: Tectonophysics, v. 623, p. 67–82, https://doi.org/10.1016/j.tecto.2014.03.019.

Miller, K.G., Kominz, M.A., Browning, J.V., Wright, J.D., Mountain, G.S., Katz, M.E., Sugarman, P.J., Cramer, B.S., Christie-Blick, N., and Pekar, S.F., 2005, The Phanerozoic record of global sea-level change: Science, v. 310, no. 5752, p. 1293–1298, https://doi.org/10.1126/science.1116412.

Pan, B., Hu, Z., Wang, J., Vandenberghe, J., Hu, X., Wen, Y., Li, Q., and Cao, B., 2012, The approximate age of the

planation surface and the incision of the Yellow River: Palaeogeography, Palaeoclimatology, Palaeoecology, v. 356, no. 9, p. 54–61, https://doi.org/10.1016/j.palaeo.2010.04.011.

Phillips, J.D., 2002, Erosion, isostatic response, and the missing peneplains: Geomorphology, v. 45, no. 3, p. 225–241, https://doi.org/10.1016/S0169-555X(01)00156-8.

Phillips, J.D., 2006, Evolutionary geomorphology: Thresholds and nonlinearity in landform response to environmental change: Hydrology and Earth System Sciences, v. 10, no. 5, p. 731–742, https://doi.org/10.5194/hess-10-731-2006.

Reynaud, J.Y., Tessier, B., Proust, J.N., Dalrymple, R., Bourillet, J.F., De Batist, M., Lericolais, G., Berne, S., and Marsset, T., 1999, Architecture and sequence stratigraphy of a late Neogene incised valley at the shelf margin, southern Celtic Sea: Journal of Sedimentary Research, v. 69, no. 2, p. 351–364, https://doi.org/10.2110/jsr.69.351.

Römer, W., 2010, Multiple planation surfaces in basement regions: Implications for the reconstruction of periods of denudation and uplift in southern Zimbabwe: Geomorphology, v. 114, no. 3, p. 199–212, https://doi.org/10.1016/j.geomorph.2009.07.001.

Rossetti, D.F., 2004, Paleosurfaces from northeastern Amazonia as a key for reconstructing paleolandscapes and understanding weathering products: Sedimentary Geology, v. 169, no. 3, p. 151–174, https://doi.org/10.1016/j.sedgeo.2004.05.003.

Song, Y., Fang, X., Torii, M., Ishikawa, N., Li, J., and An, Z., 2007, Late Neogene rock magnetic record of climatic variation from Chinese eolian sediments related to uplift of the Tibetan Plateau: Journal of Asian Earth Sciences, v. 30, no. 2, p. 324–332, https://doi.org/10.1016/j.jseaes.2006.10.004.

Song, Y., Fang, X., King, J.W., Li, J., Naoto, I., and An, Z., 2014, Magnetic parameter variations in the Chaona loess/paleosol sequences in the central Chinese Loess Plateau, and their significance for the middle Pleistocene climate transition: Quaternary Research, v. 81, no. 3, p. 433–444, https://doi.org/10.1016/j.yqres.2013.10.002.

Starkel, L., 2003, Climatically controlled terraces in uplifting mountain area: Quaternary Science Reviews, v. 22, p. 2189–2198, https://doi.org/10.1016/S0277-3791(03)00148-3.

Stinchcomb, G.E., Ese, S.G., Nordt, L.C., and Allen, P.M., 2012, A mid to late Holocene history of floodplain and terrace reworking along the middle Delaware River valley, USA: Geomorphology, v. 169–170, no. 5, p. 123–141, https://doi.org/10.1016/j.geomorph.2012.04.018.

Sun, Y., An, Z., Clemens, S.C., Bloemendal, J., and Vandenberghe, J., 2010, Seven million years of wind and precipitation variability on the Chinese Loess Plateau: Earth and Planetary Science Letters, v. 297, no. 3, p. 525–535, https://doi.org/10.1016/j.epsl.2010.07.004.

Talling P.J., and Burbank D.W., 1993, Assessment of uncertainties in magnetostratigraphic dating of sedimentary strata, *in* Aissaoui, D.M., McNeil, D.F., and Hurley, N.F., eds., Applications of Paleomagnetism to Sedimentary Geology: Society for Sedimentary Geology (SEPM) Special Publication 49, p. 59–69.

Tator, B.A., 1952, Pediment characteristics and terminology: Annals of the Association of American Geographers, v. 42, no. 4, p. 295–317, https://doi.org/10.1080/00045605209352147.

Tian, J., Wang, P., Cheng, X., and Li, Q., 2002, Astronomically tuned Plio–Pleistocene benthic $\delta^{18}O$ record from South China Sea and Atlantic-Pacific comparison: Earth and Planetary Science Letters, v. 203, no. 3, p. 1015–1029, https://doi.org/10.1016/S0012-821X(02)00923-8.

Tian, J., Zhao, Q., Wang, P., Li, Q., and Cheng, X., 2008, Astronomically modulated Neogene sediment records from the South China Sea: Paleoceanography, v. 23, no. 3, https://doi.org/10.1029/2007PA001552.

von Richthofen, F.F., 1882, China: Ergebnisse eigener Reisen und darauf gegründeter Studien, v. 2: Berlin, p. 449–451.

Wang, C.Y., Sandvol, E., Zhu, L., Lou, H., Yao, Z., and Luo, X., 2014, Lateral variation of crustal structure in the Ordos block and surrounding regions, North China, and its tectonic implications: Earth and Planetary Science Letters, v. 387, no. 1, p. 198–211, https://doi.org/10.1016/j.epsl.2013.11.033.

Wang, D.J., Wang, Y.C., Han, J.T., Duan, M.G., Shan, J.Z., and Liu, T.S., 2010, Geomagnetic anomalies recorded in L9 of the Songjiadian loess section in southeastern Chinese Loess Plateau: Chinese Science Bulletin, v. 55, no. 6, p. 520–529, https://doi.org/10.1007/s11434-009-0565-9.

Wang, N., Yang, J., Xia, Z., Mo, D., Li, Y., and Pan, M., 1996, Cenozoic deposit and tectonic geomorphology of the Shanxi graben system: Beijing, Science Press, p. 206–218 (in Chinese).

Wang, Q., Zhang, P.Z., Jeffrey, T.F., Roger, B., Kristine, M.L., Lai, X.A., You, X.Z., Niu, Z.J., Wu, J.C., Li, Y.X., Liu, J.N., Yang, Z.Q., and Chen, Q.Z., 2001, Present-day crustal deformation in continental China constrained by Global Positioning System measurements: Science, v. 294, p. 574–577, https://doi.org/10.1126/science.1063647.

Wang, Q., Li, C., Tian, G., Zhang, W., Liu, C., Ning, L., Yue, J., Cheng, Z., and He, C., 2002, Tremendous change of the earth surface system and tectonic setting of salt-lake formation in Yuncheng Basin since 7.1 Ma: Science in China, v. 45, no. 2, p. 110–122, https://doi.org/10.1007/BF02879788.

Willis, B., Blackwelder, E., and Sargent, R.H., 1907, Research in China, Part One: Descriptive Topography and Geology: Washington D.C., The Carnegie Institution of Washington, p. 3–280.

Wood, A., 1942, The development of hillside slopes: Proceedings of the Geologists' Association, v. 53, no. 3–4, p. 128–138, https://doi.org/10.1016/S0016-7878(42)80019-X.

Wu, C., 2008, Landform Environment and Its Formation in North China: Beijing, Science Press, p. 116–455 (in Chinese).

Xie, X., 2004, Discussion on rotational tectonic stress field and the genesis of circum-Ordos landmass fault system: Dizhen Xuebao, v. 17, no. 4, p. 464–472, 10.1007/s11589-004-0026-0.

Xiong, J., Li, Y., Si, S., Lv, S., Wang, Y., Zhong, Y., Xin, W., and Ci, H., 2016a, A rock fall of the north Zhongtiao Shan fault and the Yongji earthquake in 793, Shanxi Province, north China: Arabian Journal of Geosciences, v. 9, no. 18, https://doi.org/10.1007/s12517-016-2742-x.

Xiong, J., Li, Y., Zhong, Y., Si, S., and Yao, Y., 2016b, Paleomagnetism of the Jianshui basin in Yunnan, SW China, and geomorphological evolution of the Yunnan Plateau since the Neogene: Journal of Asian Earth Sciences, v. 123, p. 67–77, https://doi.org/10.1016/j.jseaes.2016.04.005.

Xiong, J., Li, Y., Zhong, Y., Si, S., Lei, J., Xin, W., Hu, X., and Yao, Y., 2017, Paleomagnetic age of the Tangxian planation surface, northwestern Zhongtiao Shan of the Shanxi Graben System, North China: Geomorphology, v. 283, p. 17–31, https://doi.org/10.1016/j.geomorph.2017.01.020.

Xu, X., Ma, X., and Deng, Q., 1993, Neotectonic activity along the Shanxi rift system, China: Tectonophysics, v. 219, no. 4, p. 305–325, https://doi.org/10.1016/0040-1951(93)90180-R.

Yang, S., and Ding, Z., 2010, Drastic climatic shift at ~2.8 Ma as recorded in eolian deposits of China and its implications for redefining the Pliocene-Pleistocene boundary: Quaternary International, v. 219, p. 37–44, https://doi.org/10.1016/j.quaint.2009.10.029.

Yang, T., Hyodo, M., Yang, Z., and Fu, J., 2004, Evidence for the Kamikatsura and Santa Rosa excursions recorded in eolian deposits from the southern Chinese Loess Plateau: Journal of Geophysical Research, D, Atmospheres, v. 109, https://doi.org/10.1029/2004JB002966.

Yang, T., Hyodo, M., Yang, Z., Ding, L., Fu, J., and Mishima, T., 2007, Early and middle Matuyama geomagnetic excursions recorded in the Chinese loess-paleosol sediments: Earth, Planets, and Space, v. 59, no. 7, p. 825–840, https://doi.org/10.1186/BF03352745.

Yang, T., Hyodo, M., Yang, Z., Ding, L., Li, H., Fu, J., Wang, S., Wang, H., and Mishima, T., 2008, Latest Olduvai short-lived reversal episodes recorded in Chinese loess: Journal of Geophysical Research, D, Atmospheres, v. 113, no. 5, p. 620–628, 10.1029/2007JB005264.

Yang, T., Hyodo, M., Yang, Z., Li, H., and Maeda, M., 2010, Multiple rapid polarity swings during the Matuyama-Brunhes transition from two high-resolution loess-paleosol records: Journal of Geophysical Research, Solid Earth, v. 115, B5, 10.1029/2009JB006301.

Zachos, J., Pagani, M., Sloan, L., Thomas, E., and Billups, K., 2001, Trends, rhythms, and aberrations in global climate 65 Ma to present: Science, v. 292, no. 5517, p. 686–693, https://doi.org/10.1126/science.1059412.

Zhai, M.G., Santosh, M., and Zhang, L., 2011, Precambrian geology and tectonic evolution of the North China Craton: Gondwana Research, v. 20, p. 1–5, https://doi.org/10.1016/j.gr.2011.04.004.

Zhang, P., Burchfiel, B.C., Molnar, P., Zhang, W., Jiao, D., Deng, Q., Wang, Y., Leigh, R., and Song, F., 1991, Amount and style of Late Cenozoic Deformation in the Liupan Shan Area, Ningxia Autonomous Region, China: Tectonics, v. 10, no. 6, p. 1111–1129, https://doi.org/10.1029/90TC02686.

Zhang, P., Molnar, P., and Downs, W.R., 2001, Increased sedimentation rates and grain sizes 2–4 Myr ago due to the influence of climate change on erosion rates: Nature, v. 410, p. 891–897, https://doi.org/10.1038/35073504.

Zhao, B., Zhang, C., Wang, D., Huang, Y., Tan, K., Du, R., and Liu, J., 2017, Contemporary kinematics of the Ordos block, North China and its adjacent rift systems constrained by dense GPS observations: Journal of Asian Earth Sciences, v. 135, p. 257–267, https://doi.org/10.1016/j.jseaes.2016.12.045.

Zhu, Y., Zhou, L., Mo, D., Kaakinen, A., Zhang, Z., and Fortelius, M., 2008, A new magnetostratigraphic framework for late Neogene Hipparion Red Clay in the eastern Loess Plateau of China: Palaeogeography, Palaeoclimatology, Palaeoecology, v. 268, no. 1, p. 47–57, https://doi.org/10.1016/j.palaeo.2008.08.001.

MANUSCRIPT RECEIVED 22 NOVEMBER 2017
REVISED MANUSCRIPT RECEIVED 17 FEBRUARY 2018
MANUSCRIPT ACCEPTED 13 APRIL 2018